About an autoconvolution problem arising in ultrashort laser pulse characterization

S. Bürger

Preprint 2014-16

Preprintreihe der Fakultät für Mathematik
ISSN 1614-8835

ABOUT AN AUTOCONVOLUTION PROBLEM ARISING IN ULTRASHORT LASER PULSE CHARACTERIZATION

STEVEN BÜRGER

Abstract. We are investigating a kernel-based autoconvolution problem, which has its origin in the physics of ultra short laser pulses. The task in this problem is to reconstruct a complex-valued function x on a finite interval from measurements of its absolute value and a kernel-based autoconvolution of the form

$$[F(x)](s) = \int k(s,t)x(s-t)x(t)\mathrm{d}t.$$

This problem has not been studied in the literature. One reason might be that one has more information than in the classical autoconvolution case, where only the right hand side is available. Nevertheless we show that ill posedness phenomena may occur. We also propose an algorithm to solve the problem numerically and demonstrate its performance with artificial data. Since the algorithm fails to produce good results with real data and we suspect that the data for $|F(x)|$ are not dependable we also consider the whole problem with only $\arg(F(x))$ given instead of $F(x)$.

1. Introduction

The so-called self-diffraction SPIDER (SD-SPIDER) was introduced by Sebastian Koke, Simon Birkholz, Jens Bethge, Christian Grebing and Günter Steinmeyer from Max Born Institute for Nonlinear Optics and Short Pulse Spectroscopy, Berlin ([11]). The aim of this method is the reconstruction of the electric field $E(t)$ of ultra-short laser pulses, which, in the simplest case, can be considered as a real-valued function of time. It is usually decomposed into an amplitude part and an oscillating part by

$$E(t) = \sqrt{I(t)}\cos\{\omega_0 t + \varphi(t)\} \tag{1.1}$$

where $I(t)$ is the intensity, ω_0 the carrier frequency and $\phi(t)$ is called temporal phase. Since measurements are available only for the spectral

Date: October 16, 2014.

2010 *Mathematics Subject Classification.* 47J06, 78A60, 65J20.

Key words and phrases. Autoconvolution equation, inverse problems, local well-posedness and ill-posedness.

domain we have to consider the Fourier transform of $E(t)$

$$\hat{E}(\omega) := [\mathcal{F}(E)](\omega) = \frac{1}{\sqrt{2\pi}} \int_{-\infty}^{\infty} E(t) e^{-i\omega t} \mathrm{d}t \tag{1.2}$$

This is a complex-valued function and hence it can be written in polar coordinates

$$\hat{E}(\omega) = \sqrt{S(\omega)} \exp\{i\phi(\omega)\} \tag{1.3}$$

where $S(\omega)$ is the spectrum and $\phi(\omega)$ is called spectral phase. Fortunately one is able to measure the spectrum directly. Hence determination of the spectral phase would be sufficient to obtain the desired quantity $E(t)$ by inverse Fourier transform. To this end the physicists generate so-called SD-pulses. The electric field of these pulses in the spectral domain $\hat{E}_{SD}(\omega)$ is related to $\hat{E}(\omega)$ through the following equation

$$\hat{E}_{SD}(\omega) = \int_{0}^{\omega+\omega_{cw}} K(\omega, \tau) \hat{E}(\omega + \omega_{cw} - \tau) \hat{E}(\tau) \mathrm{d}\tau \tag{1.4}$$

Here ω_{cw} is a constant which can be measured and $K(\omega, \tau)$ is a kernel function which is smooth in ω and τ. We also write $\hat{E}_{SD}$ in polar coordinates as

$$\hat{E}_{SD}(\omega) = \sqrt{S_{SD}(\omega)} \exp\{i\phi_{SD}(\omega)\} \tag{1.5}$$

Again one can measure the spectrum of $\hat{E}_{SD}$, but for physical reason this measurement is not very reliable. The advantage is now that the spectral phase of $\hat{E}_{SD}$ can be calculated from measurements of a so-called SD-interferogram and a fundamental interferogram. The measurement setup for the SD-interferogram is shown in the following picture

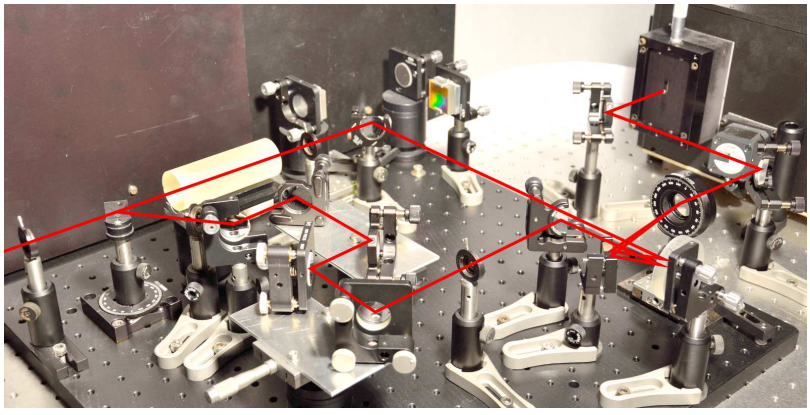

For physical details we refer to [6] and [7].
The measurements for the spectrum of $\hat{E}$ show that it vanishes outside a compact interval $[\omega_l, \omega_u]$, which means

$$\text{supp } \hat{E} \subset [\omega_l, \omega_u]. \tag{1.6}$$

Consequently $\hat{E}_{SD}$ vanishes outside the interval $[2\omega_l - \omega_{cw}, 2\omega_u - \omega_{cw}]$.

$$\text{supp } \hat{E}_{SD} \subset [2\omega_l - \omega_{cw}, 2\omega_u - \omega_{cw}] \tag{1.7}$$

Thus, formula (1.4) can be written as

$$\hat{E}_{SD}(\omega) = \int_{\max\{\omega_l, \omega+\omega_{cw}-\omega_u\}}^{\min\{\omega_u, \omega+\omega_{cw}-\omega_l\}} K(\omega,\tau)\hat{E}(\omega+\omega_{cw}-\tau)\hat{E}(\tau)\mathrm{d}\tau \tag{1.8}$$

With the substitutions

$$\begin{aligned} y(s) :=& \hat{E}_{SD}(-\omega_{cw} + 2\omega_l + s(\omega_u - \omega_l)) \\ x(t) :=& \hat{E}(\omega_l + t(\omega_u - \omega_l)) \\ k(s,t) :=& K(-\omega_{cw} + 2\omega_l + s(\omega_u - \omega_l), \omega_l + t(\omega_u - \omega_l)) \end{aligned}$$

equation 1.8 turns to

$$[F(x)](s) := y(s) = \int_{\max\{0, s-1\}}^{\min\{1,s\}} k(s,t)x(s-t)x(t)\mathrm{d}t \qquad 0 \le s \le 2 \tag{1.9}$$

where we consider F as an operator

$$F : L^2_{\mathbb{C}}(0,1) \to L^2_{\mathbb{C}}(0,2)$$

and assume that $k \in L^\infty\big([0,2] \times [0,1]\big)$. The problem is now the following: Given k and noisy data for $|x|$ and y the phase $\arg(x)$ is to be determined. We already mentioned that the data for $|y|$ are rather not reliable and therefore we will also consider the problem where we only have measurements for $|x|$ and $\arg(y)$ given.

Now the paper is organized as follows: in Section 2 we give some ill- and well-posedness results about the considered problem. In Section 3 we develop one algorithm for each problem setting and we test these algorithms with artificial data. The behavior of the algorithms with real data is the content of Section 4. Finally, in Section 5 we summarize our results.

2. Theoretical results

In this section we investigate properties of the operator equation (1.9). For $k \equiv 1$ the operator F defined in this equation turns to

$$[F(x)](s) = \int_{\max\{0, s-1\}}^{\min\{1,s\}} x(s-t)x(t)\mathrm{d}t \qquad 0 \le s \le 2 \tag{2.1}$$

and the corresponding operator equation

$$[F(x)](s) = y(s) \qquad 0 \leq s \leq 2 \tag{2.2}$$

is the standard autoconvolution equation with data on $[0, 2]$. A study of this equation had already been published in [4]. Beyond there are some papers that are dealing with the operator equation

$$F : L^2_{\mathbb{R}}(0,1) \to L^2_{\mathbb{R}}(0,1), \quad [F(x)](s) = \int_0^s x(s-t)x(t)\mathrm{d}t. \tag{2.3}$$

See for instance [2], [8] and [10].

For our further considerations we will need the term of local ill-posedness. The definition of ill-posedness of a nonlinear problem is not as clear as in the linear case. Therefore, we recall the following definition first published in [9, Definition 2].

Definition 2.1. *Let X and Y be Banach spaces. We call a nonlinear operator equation*

$$G : \mathcal{D}(G) \subset X \to Y, \quad G(x) = y \tag{2.4}$$

locally well-posed at a solution point $x^\dagger \in \mathcal{D}(G)$ if there is a closed ball $\overline{B}_r(x^\dagger) := \{x \in X : \|x - x^\dagger\| \leq r\}$ around $x^\dagger$ with radius $r > 0$ such that, for every sequence $\{x_n\}_{n=1}^\infty \subset \overline{B}_r(x^\dagger) \cap \mathcal{D}(G)$, the limit condition $\lim_{n\to\infty} \|G(x_n) - G(x^\dagger)\| = 0$ implies that $\lim_{n\to\infty} \|x_n - x^\dagger\| = 0$. Otherwise the equation is called locally ill-posed at $x^\dagger \in \mathcal{D}(G)$, which means that, for arbitrarily small radii $r > 0$, there exist sequences $\{x_n\}_{n=1}^\infty \subset \overline{B}_r(x^\dagger) \cap \mathcal{D}(G)$ such that $\lim_{n\to\infty} \|G(x_n) - G(x^\dagger)\| = 0$, but $\limsup_{n\to\infty} \|x_n - x^\dagger\| > 0$.

The following example was alredy mentioned in [2, Example 3.2.] and shows the ill-posedness of the operator equation (2.1)

Example 2.2. *For $r > 0$ let $z_n \in L^2(0,1)$ be defined as $z_n := re^{in^2t^2}$. Then it is easy to show that $z_n \rightharpoonup 0$, $z_n * z_n \to 0$ and $||z_n|| = r$, where $x_1 * x_2$ denotes the convolution of x_1 and x_2. Now for arbitrary $x \in L^2_{\mathbb{C}}(0,1)$ we define $x_n := x + z_n$ and it follows that*

$$F(x_n) - F(x) = 2x * z_n + z_n * z_n \to 0$$

but

$$||x_n - x|| = ||z_n|| = r$$

Thus the operator equation 2.1 is locally ill-posed at any point $x \in L^2(0,1)$.

Note that that the sequence (z_n) is bounded in the sense that

$$\max_{t\in[0,1]} z(t) = r.$$

This example can also be used to show that the operator equation

$$F : C(0,1) \to C(0,2), \tag{2.5}$$

$$[F(x)](s) := y(s) = \int_{\max\{0,s-1\}}^{\min\{1,s\}} x(s-t)x(t)\mathrm{d}t \qquad 0 \le s \le 2 \tag{2.6}$$

is locally ill-posed everywhere. Here $C(a,b)$ denotes the space of continous complex-valued functions on $[a,b]$.

On the other hand there are locally well-posed situations if the amplitude function is known exactly. This is shown by the next proposition, which already appeard in [2, Proposition 3.3.].

Proposition 2.3. *Let $a \in L^\infty_{\mathbb{R}}(0,1)$, $a \not\equiv 0$ be the amplitude function of the exact solution x of (2.1). If we restrict the domain of the operator F to*

$$\mathcal{D}(F) := \{a(t)e^{i\phi(t)} \,|\, 0 \le t \le 1,\ \phi : [0,1] \to \mathbb{R}\}$$

then there exist phase functions $\phi^\dagger$ such that this problem is locally well posed at $x^\dagger$ where $x^\dagger(t) := a(t)e^{i\phi^\dagger(t)}$.

Up to this moment we summarized results for the situation with full data given, which means that measurements for absolute value and phase of the right hand side of (2.2). Now we come to the completely new situation where the absolute value of the right hand side $|y|$ is not available and we have to consider a new operator which reflects this situation. To this end we define

$$\tilde{F} : \mathcal{D}(\tilde{F}) \subset L^2_{\mathbb{C}}(0,1) \to Y, \tag{2.7}$$

$$[\tilde{F}(x)](s) = \begin{cases} \arg\big([F(x)](s)\big) & \text{for } [F(x)](s) \neq 0 \\ 0 & \text{for } [F(x)](s) = 0 \end{cases} \tag{2.8}$$

where

$$Y := \{\Psi : [0,2] \to [0,2\pi) \,|\, \Psi \text{ measurable}\}, \tag{2.9}$$

becomes a metric space with the metric

$$d(\Psi,\Phi)^2 = \int_0^2 (1 - \cos(\Psi(t) - \Phi(t)))\mathrm{d}t \tag{2.10}$$

In this setting we get the following result

Theorem 2.4. *Let $k \equiv 1$ and $a \in L^2_{\mathbb{R}}(0,1)$, $a \not\equiv 0$ be the amplitude function of the exact solution $x \in L^2_{\mathbb{C}}(0,1)$ and let $F(x) \neq 0$ a.e.. If we restrict the domain of the operator $\tilde{F}$ to*

$$D := \{a(t)e^{i\phi(t)} \,|\, 0 \le t \le 1,\ \phi : [0,1] \to \mathbb{R}\}$$

then the operator equation is locally ill-posed at any point $x \in D$.

Our proof for Theorem 2.4. is long and rather technical, so we just give a sketch of it here.
Sketch of a proof: Let μ denote the Lebesgue measure on the measureable space $(\mathbb{R}, \mathcal{B})$, where $\mathcal{B}$ is the Borel-σ-algebra on $\mathbb{R}$. For $y \in L^2_{\mathbb{C}}(0,2)$ we define

$$\psi_y(t) := \mu(\{|y| \leq t\})$$

With the dominated convergence theorem it is easy to show that

$$\lim_{t \to 0} \psi_y(t) = \mu(\{y = 0\})$$

If now $\mu(\{y = 0\}) = 0$ and $\tilde{y} \in L^2_{\mathbb{C}}(0,2)$ one can prove that $||\tilde{y} - y|| \leq \delta$ implies

$$|| \arg \tilde{y} - \arg y|| \leq \sqrt{2\big(\delta + \psi_y(\sqrt{\delta})\big)} \tag{1}$$

Another important technical argument is the following: for $y_1, y_2 \in L^2_{\mathbb{C}}(0,2)$ and $0 < t_1 < t_2$ we have

$$\psi_{y_1}(t_1) \leq \psi_{y_2}(t_2) + \frac{\sqrt{2}||y_2 - y_1||}{t_2 - t_1} \tag{2}$$

Let now $x \in L^2_{\mathbb{C}}(0,1)$ such that $\mu(\{F(x) = 0\}) = 0$. We choose a sequence $(\bar{x}_n)_{n \in \mathbb{N}}$ of step functions with equispaced discontinuities

$$\bar{x}_n = \sum_{k=1}^{m_n} c_n^k \chi_{[\frac{k-1}{m_n}, \frac{k}{m_n}]} \tag{3}$$

such that $||x - \bar{x}_n|| \leq 2^{-n}$. Let $\epsilon < \frac{1}{14}$. Now, for each $\bar{x}_n$ we define a sequence x_n^l by

$$x_n^k(t) := \sum_{l=1}^{m_n} c_n^l z_k(m_n t - l + 1)$$

where m_n and c_n^k are the same as in (3) and

$$z_k(t) := \begin{cases} 1 & \text{for } 0 \leq t \leq \frac{1}{2} - \epsilon \text{ or } \frac{1}{2} + \epsilon < t \leq 1 \\ \exp\left(\frac{i\pi k^2}{2\epsilon}\left(t - \frac{1}{2} + \epsilon\right)^2\right) & \text{for } \frac{1}{2} - \epsilon < t \leq \frac{1}{2} + \epsilon \\ 0 & \text{else} \end{cases}$$

Using (1) one can show that

$$\arg F(x_n^k) \to \arg F(\bar{x}_n) \quad \text{ as } k \to \infty$$

We choose $p \in \mathbb{N}$ such that

$$|| \arg F(x_n^p) - \arg F(\bar{x}_n)|| \leq 2^{-n}$$

and define x_n by $|x_n| := |x|$ and $\arg x_n := \arg x_n^p$. With (1) and (2) at hand one shows that

$$\arg x_n \to \arg x \quad \text{ as } n \to \infty$$

However, using the triangle inequality it is easy to see that

$$\lim_{n\to\infty} ||x_n - x|| \to 2\sqrt{\epsilon}||x|| > 0$$

This also shows that for given $r > 0$ one can choose ϵ small enough such that $||x_n - x|| \leq r$ for all $n \geq n_0$ for some $n_0 \in \mathbb{N}$. Thus the operator equation is ill-posed at x.

3. Numerical solution and examples

In this section we propose a numerical procedure to solve the reconstruction problem for both cases of given data. For papers about numerical methods for operator equations of autoconvolution type see for example [1], [3], [5] and [10]. Since the results of the last section show that ill-posedness phenomena can occur, we have to use a regularization technique. The most important question is how to bring the measurement of the amplitude function into play. First we assume that measurements a_ρ for the amplitude function $a = |x|$ and y_δ for the right hand side y are available such that

$$||a_\rho - a|| \leq \rho \qquad ||y - y_\delta|| \leq \delta \tag{3.1}$$

Now we consider the functional

$$T_\alpha(x) = \alpha\big|\big||x| - a_\rho\big|\big|^2 + ||F(x) - y_\delta||^2 \tag{3.2}$$

The first summand penalizes the deviation of a_ρ and a while the second one is a residual term known from Tikhonov regularization. α is a coupling constant but no regularization parameter in the classical sense since a high value of α does not imply a high regularization, especially if ρ is big. We want to approximate a minimizer of this functional by a gradient method.
Since T_α is not holomorphic we replace x by $c + id$ with $c, d \in L^2_{\mathbb{R}}(0,1)$ and get

$$T_\alpha(c,d) = \alpha\big|\big|\sqrt{c^2+d^2} - a_\rho\big|\big|^2 + ||F(c+id) - y_\delta||^2$$

$$[\nabla_c T_\alpha](c,d) = 2\alpha c\left(1 - \frac{a_\rho}{\sqrt{c^2+d^2}}\right) + 2F_c'^*(c,d)\,(F(c,d) - y_\delta)$$

$$[\nabla_d T_\alpha](c,d) = 2\alpha d\left(1 - \frac{a_\rho}{\sqrt{c^2+d^2}}\right) + 2F_d'^*(c,d)\,(F(c,d) - y_\delta)$$

where

$$F(c,d) = \int_{\max\{0,s-1\}}^{\min\{1,s\}} k(s,t)(c(s-t) + id(s-t))(c(t) + id(t))\mathrm{d}t$$

and

$$[F_c'^*(c,d)h](t) = \int_t^{t+1} (k(s,t) + k(s,s-t))(c(s-t) + id(s-t))h(s)\mathrm{d}s$$

$$[F_d'^*(c,d)h](t) = \int_t^{t+1} (k(s,t) + k(s,s-t))(ic(s-t) - d(s-t))h(s)\mathrm{d}s$$

Our numerical procedure starts with the function $x_0 := a_\rho$, which means that $c_0 := a_\rho$ and $d_0 := 0$. While the expression

$$||[\nabla_c T_\alpha](c_n, d_n)||^2 + ||[\nabla_d T_\alpha](c_n, d_n)||^2$$

is greater than some constant κ for the current point $x_n = c_n + id_n$ we add a negative multiple of the gradient $t[\nabla_c T_\alpha](c_n, d_n)$ to c_n and analogously for d_n. The step size t is calculated numerically. In compact form the algorithm looks as follows:

- SET $c_0 = x_0 := a_\rho$, $d_0 := 0$, $n = 0$
- WHILE $||[\nabla_c T_\alpha](c_n, d_n)||^2 + ||[\nabla_d T_\alpha](c_n, d_n)||^2 \geq \kappa$
  - CALCULATE
    $t_{min} = \arg\min_{t>0} T_\alpha \left(c_n - tg_n^c, d_n - tg_n^d\right)$
  - SET $c_{n+1} := c_n - t_{min} g_n^c$, $d_{n+1} := d_n - t_{min} g_n^d$, $n := n + 1$

For a realization of this algorithm one has to discretize. In our computations we used piecewise constant basis function to approximate x and k. For $n \in \mathbb{N}$ let

$$x(t) \approx \sum_{i=1}^{N} x^i e_i(t) \tag{3.3}$$

$$k(s,t) \approx \sum_{i=1}^{N} \sum_{j=i}^{N+i-1} k^{ji} \cdot g_{ji}(s,t) \tag{3.4}$$

where

$$e_i := \sqrt{N} \chi_{[\frac{i-1}{N}, \frac{i}{N}]}$$

in which $\chi_{[\frac{i-1}{N}, \frac{i}{N}]}$ denotes the characteristic function of the interval $[\frac{i-1}{N}, \frac{i}{N}]$ and

$$g_{ji}(s,t) := \begin{cases} 1 & \text{for } \frac{i-1}{N} \leq t \leq \frac{i}{N} \wedge \frac{2j-1}{2N} \leq s \leq \frac{2j+1}{2N} \\ 0 & \text{else} \end{cases}$$

The reason for the choice of these non-smooth basis functions is the simple structure of the operator F in this case. If we assume that the kernel $k(s,t)$ is smooth and has a bounded first derivative with respect to s, which implies that $k^{(j+1)\,i} - k^{ji}$ is small for N sufficiently large,

we get the following approximation

(3.5)

$$\begin{aligned}[F(x)](s) &= \int_{\max\{0,s-1\}}^{\min\{1,s\}} k(s,t)x(s-t)x(t)\mathrm{d}t \\ &= N\sum_{k,l=1}^{N} x^k x^l \int_{\max\{0,s-1\}}^{\min\{1,s\}} k(s,t)\chi_{[\frac{k-1}{N},\frac{k}{N}]}(s-t)\chi_{[\frac{l-1}{N},\frac{l}{N}]}(t)\mathrm{d}t \\ &\approx \sum_{k,l=1}^{N} x^k x^l k^{(k+l-1)\,l} h_{k+l-1}(s)\end{aligned}$$

where

$$h_{k+l-1}(s) := h(Ns-k-l+1)$$

and

$$h(s) := \begin{cases} s & \text{for } -1 \le s+1 < 0 \\ 2-s & \text{for } 0 \le -s+1 < 1 \\ 0 & \text{else} \end{cases}$$

is a hat function. Hence we take (h_j), $j = 1, \ldots, 2N-1$ as basis functions in $L^2(0,2)$. For the scalar products in $L^2(0,1)$ and $L^2(0,2)$ with respect to the chosen basis functions we have

$$\langle e_k, e_l \rangle = \delta_{kl}$$

and

$$\langle h_k, h_l \rangle = \frac{2}{3N}\big(\delta_{kl} + \tfrac{1}{4}(\delta_{(k-1)l} + \delta_{(k+1)l})\big)$$

In our numerical examples we choose $N = 100$ and for the parameters in the algorithm we set $\kappa = 10^{-9}$ and $\alpha = 0.05$.
For the artificial data we use pointwise Gauss-distributed noise with $\rho = 0.01||x^\dagger||$ and $\delta = 0.05||y||$. This is approximately what we also would expect for real data. The diagram on the left shows the exact and the reconstructed amplitude function whereas the diagram on the left shows the exact and the reconstructed phase function. The exact functions are plotted in red and the reconstructed ones in blue.
The first test function is a very simple function given by

$$a \equiv 1 \qquad \phi(t) = 6t \qquad k \equiv 1$$

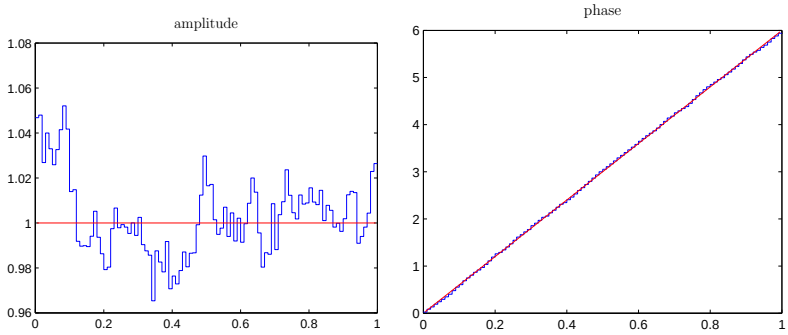

The second test function has quadratic amplitude and phase and the kernel is again constant

$$a(t) = 1 - 3(t - \tfrac{1}{2})^2 \qquad \phi(t) = 6t^2 \qquad k \equiv 1$$

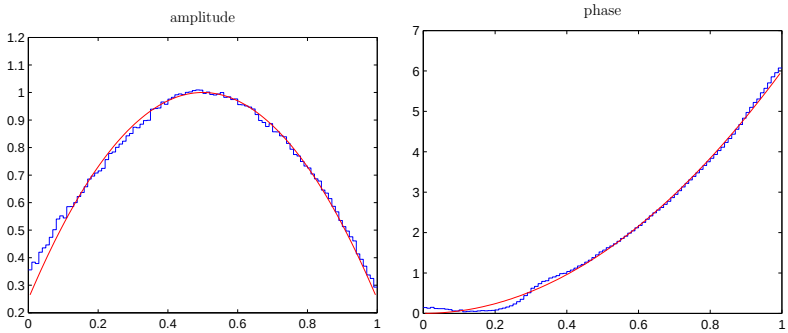

Our last test function has a Gaussian function as amplitude and an exponential phase. The kernel here is a quadratic function.

$$a(t) = \exp\big(-10(t - \tfrac{1}{2})^2\big) \qquad \phi(t) = e^{3t} \qquad k(s,t) = 1 + \tfrac{1}{4}(s^2 + t^2)$$

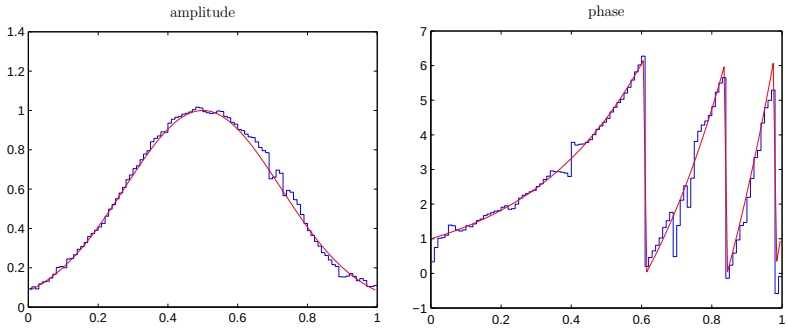

Now we come to our second problem, namely the one where only a_ρ and $\arg(y_\delta)$ are given. Here we consider the functional

$$S_\alpha(x) := \alpha\big|\big|a - |x|\big|\big|^2 + \frac{1}{||F(x)||^2}\big|\big|F(x) - |F(x)| \cdot e^{i\Psi}\big|\big|^2 \tag{3.6}$$

Note that the norms in this functional are exclusively L^2-norms. The factor $\frac{1}{||F(x)||^2}$ is important to avoid ill-posedness phenomena. Apart

from the functional the setting is the same as in the full data case. For our numerical studies we set again $N = 100$ and $\kappa = 10^{-9}$, but $\alpha = 0.5$. The noise is unchanged. We get the following reconstructions

$a \equiv 1 \qquad \phi(t) = 6t \qquad k \equiv 1$

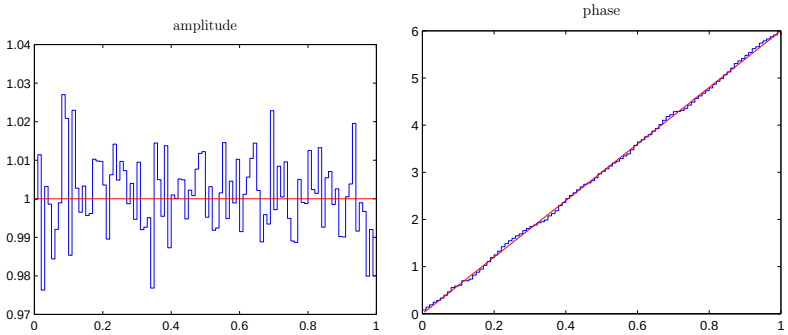

$a(t) = 1 - 3(t - \frac{1}{2})^2 \qquad \phi(t) = 6t^2 \qquad k \equiv 1$

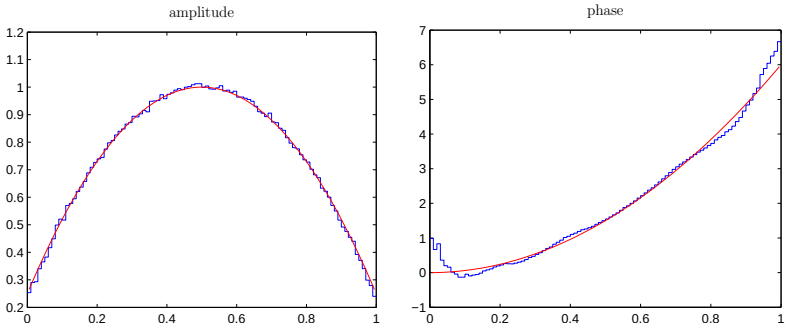

$a(t) = \exp\big(-10(t - \frac{1}{2})^2\big) \qquad \phi(t) = e^{3t} \qquad k(s,t) = 1 + \frac{1}{4}(s^2 + t^2)$

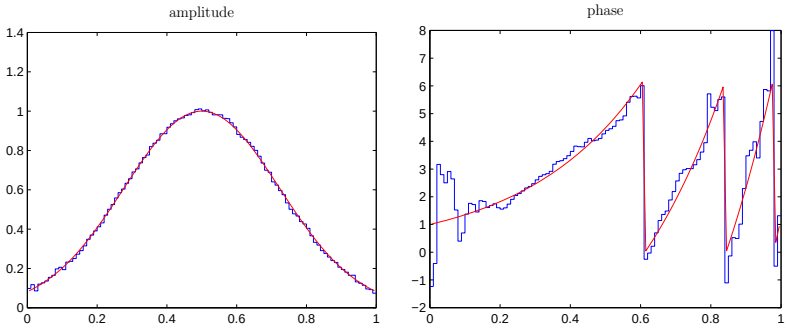

The following table shows the relative errors of the reconstructions. If x is the true solution and x_r denotes the reconstructed one then the relative error of the reconstruction is $\mu = \frac{||x - x_r||}{||x||}$.

As one can see looking at the relative errors, the reconstructions with only phase information about y are only slightly worse than the ones with full data. This is somehow surprising, especially in view of the theoretical results in Section 2.

test function	1	2	3
full data	0.0266	0.0764	0.2341
only phase	0.0411	0.1123	0.2736

TABLE 1. relative errors μ for reconstructed functions.

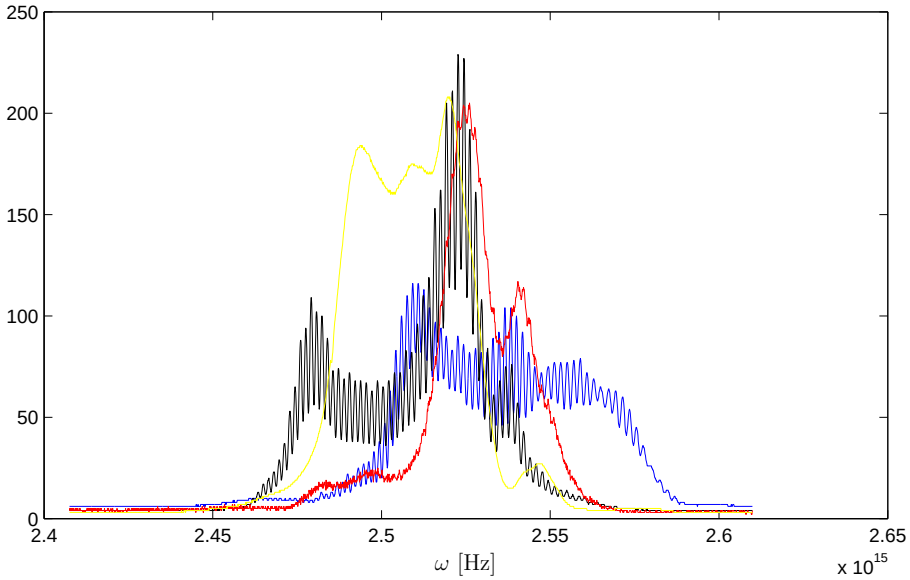

FIGURE 1. measured data, red: spectrum of fundamental pulse $\sqrt{S(\omega)}$, yellow: spectrum of SD-pulse $\sqrt{S_{SD}(\omega)}$, blue: SD-interferogram, black: fundamental interferogram

4. Application to real data

Now we want to apply our method introduced in the last Section to real data which come from measurements with SD-SPIDER. The spectrometer can measure frequencies in the interval $[2.408 \cdot 10^{15} Hz, 2.610 \cdot 10^{15} Hz]$ and we have $\omega_{cw} \approx 2.532$. The measured data are plotted in Figure 1. Here the spectra of original and SD-pulse $\sqrt{S}$ and $\sqrt{S_{SD}}$ correspond to $|x|$ and $|y|$ respectively, whereas SD-interferogram and fundamental interferogram are needed to reconstruct the phase $\arg(y)$. In view of $\sqrt{S(\omega)}$ we set $\omega_l = 2.469$ and $\omega_u = 2.576$. For the phase of the SD-pulse $\phi_{SD}(\omega)$ we get the reconstruction shown in Figure 2. Note that the information in the middle part of ϕ_{SD} is most important, since the spectrum attains its maximum there. Finally we need to know the kernel K, which is shown in Figure 3. For the reconstruction with real data we use $N = 1000$ basis functions in $L^2_{\mathbb{C}}(0,1)$ (cf. (3.3)). The reconstruction in the full data case failed completely (see Figure 4) since the reconstructed amplitude is far away from the measured one. The reason could be that $|\hat{E}_{SD}|$ does not match with $|\hat{E}|$ and ω_{cw} since in

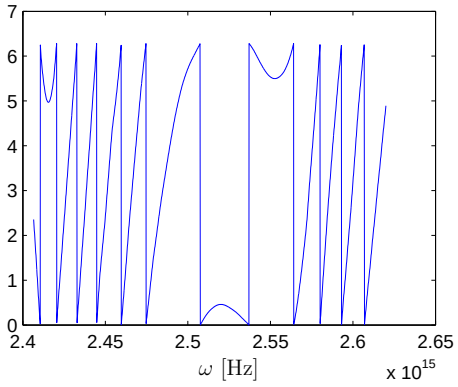

FIGURE 2. SD-phase $\phi_{SD}(\omega)$

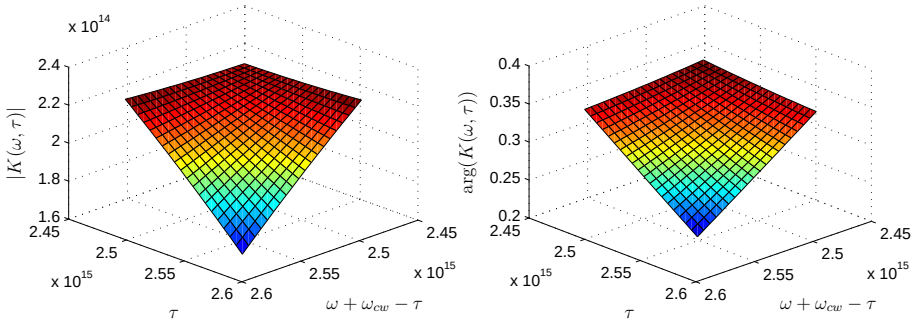

FIGURE 3. absolute value and phase of the Kernel function K

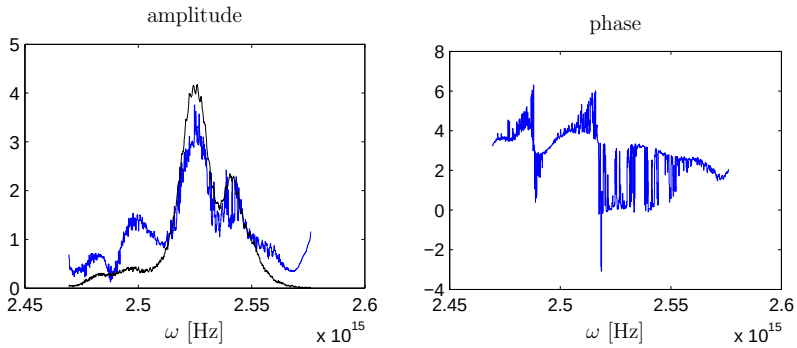

FIGURE 4. reconstruction with full data. Left side: measured amplitude (black) and reconstructed amplitude (blue). Right side: reconstructed phase

view of (1.7) the support of $|\hat{E}_{SD}|$ seems to be too far left. From the physical point of view the measurement of $|\hat{E}_{SD}|$ shows big fluctuations in time and is therefore not faithful. In the reconstruction where only phase information about $\hat{E}_{SD}$ was used (see Figure 5), the result looks much better since there are fewer oscillations in amplitude and phase

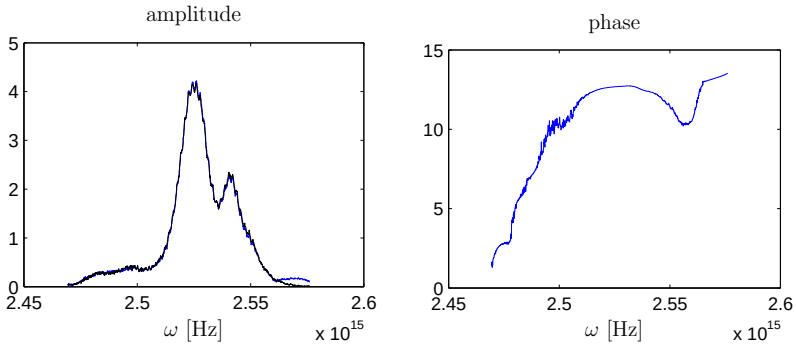

FIGURE 5. reconstruction with phase only. Left side: measured amplitude (black) and reconstructed amplitude (blue). Right side: reconstructed phase

function. Especially in the interval $[1.51 \cdot 10^{15} Hz, 1.55 \cdot 10^{15} Hz]$ the reconstructed phase does not show any oscillations. This is the most important part of the reconstruction since only on this interval the amplitude function is not close to zero.

5. CONCLUSIONS

We have seen that the complex autoconvolution problems, which we investigated here, are ill-posed and hence regularization is required. In comparison to [6] and [7] also a new measurement situation was considered, where fewer data are required. Numerical studies have shown that our regularization approach yields good results with artificial data. For real data we have first results which can be interpreted by physicists.

REFERENCES

[1] Bürger S, Flemming J: Deautoconvolution: a new decomposition approach versus TIGRA and local regularization. *J. Inverse and Ill-Posed Problems*. Published online 18 April 2014: DOI 10.1515/jiip-2013-0082

[2] Bürger S, Hofmann B: About a deficit in low-order convergence rates on the example of autoconvolution. *Applicable Analysis*. Published online 19 February 2014:
`http://www.tandfonline.com/doi/full/10.1080/00036811.2014.886107`

[3] Dai Z, Lamm, P K: Local regularization for the nonlinear inverse autoconvolution problem. *SIAM J. Numer. Anal.* **46** (2008), 832–868.

[4] Fleischer G, Hofmann B: On inversion rates for the autoconvolution equation. *Inverse Problems* **4** (1996), 419–435.

[5] Flemming J: Regularization of autoconvolution and other ill-posed quadratic equations by decomposition. *J. Inverse and Ill-Posed Problems* **22** (2014), 551-567.

[6] Gerth D: Regularization of an autoconvolution problem occuring in measurements of ultra-short laser pulses. *Diploma thesis* Chemnitz 2011
`http://nbn-resolving.de/urn:nbn:de:bsz:ch1-qucosa-85485`

[7] D. Gerth, B. Hofmann, S. Birkholz, S. Koke, G. Steinmeyer: Regularization of an autoconvolution problem in ultrashort laser pulse characterization. *Inverse Problems in Science and Engineering* **22** (2014), 245–266.

[8] Gorenflo R, Hofmann B: On autoconvolution and regularization. *Inverse Problems* **2** (1994), 353–373.
[9] Hofmann B, Scherzer O: Factors influencing the ill-posedness of nonlinear problems. *Inverse Problems* **6** (1994), 1277–1297.
[10] Janno J: Lavrent'ev regularization of ill-posed problems containing nonlinear near-to-monotone operators with application to atoconvolution equation. *Inverse Problems* **16** (2000), 333–348.
[11] Koke S, Birkholz S, Bethge J, Grebing C, Steinmeyer G: Self-diffraction SPIDER. *Conference on Lasers and Electro-Optics, OSA Technical Digest (CD) (Optical Society of America)* 2010, Paper CMK3, DOI 10.1364/CLEO.2010.CMK3.

Faculty of Mathematics, TU Chemnitz, 09107 Chemnitz, Germany
E-mail address: steven.buerger@mathematik.tu-chemnitz.de